Blockwise Classification of Lung Patterns in Unsegmented CT Images

Luiza D. Bagesteiro, Lucas F. Oliveira and Daniel Weingaertner
Vision, Robotics and Images Research Group (VRI), Department of Informatics
Federal University of Parana (UFPR), Curitiba, Brazil
{*ldbagesteiro, lferrari, danielw*}*@inf.ufpr.br*

***Abstract*—Diagnosis of lung diseases is usually accomplished by detecting abnormal characteristics in Computed Tomography (CT) scans. We report an initial study for classifying texture patterns in High-Resolution lung CTs using the Completed Local Binary Pattern (CLBP) descriptor with a Support Vector Machine (SVM). The main contribution of the proposed method is that it does not depend on a previously segmented lung, as it performs a coarse segmentation by classifying body areas outside the lungs. The classified patterns are: non lung, normal lung tissue, emphysema, ground-glass opacity, fibrosis and micronodules. Using image blocks of 32×32 pixels, extracted from a public dataset with 113 patients, correct blockwise classification of non lung patterns was achieved with an accuracy of 98.91%. Regarding normal and pathological lung patterns, a mean accuracy of 91.81% was obtained. This is similar to the reported results in literature which used a pre-segmented lung.**

***Keywords*-lung diseases; lung segmentation; Completed Local Binary Pattern; High-Resolution Computed Tomography.**

I. Introduction

Diagnosis of lung diseases is usually accomplished by detecting abnormal characteristics in Computed Tomography (CT) scans. The visual patterns or image textures of these characteristics have valuable information about the nature of the abnormality, especially when there is a prior knowledge relating patterns to diseases. The application of image processing techniques can increase the confidence and consistency of diagnosis [1] by providing quantitative values for the form and/or texture of the CT image characteristics, which in turn can be used with pattern recognition algorithms to classify them according to predefined classes.

Image classification is performed in three steps [2]: the first is image acquisition by acquiring equipment. The second step involves image preprocessing, segmentation and features extraction. The relevant information is obtained by extracting and quantifying features that allow an assignment of images to different classes. One approach is to extract features using textures. Finally the third step uses a classifier algorithm, (e.g. Support Vector Machines (SVM) or Neural Networks), to classify and quantify the extracted features.

In recent years, many studies about classification of lung diseases have been developed, but the different resolution techniques show that there is still no consensus about what features should be used in the classification process. Usually, pulmonary patterns are associated to texture properties [3]. The studies have shown difficulty in differentiating certain pulmonary patterns, which also cause confusion among specialists [4] due to its similarity, showing that this is the main problem to be faced. Moreover, the segmentation of lungs affected by high density pathologies is still an ongoing work [1], and most studies about classification of lung diseases use images of the lungs which are already segmented [5]–[10]. In other cases, a semiautomatic segmentation is applied [11].

The main goal of our research is to execute an analysis and quantification of lung disease patterns in High-Resolution Computed Tomography (HRCT) images, performing a coarse lung segmentation by also classifying body areas outside the lungs. Based on that, this paper presents initial results in the classification of image blocks of the following texture patterns: non-lung (e.g. bone, tissue and fat), normal lung tissue, emphysema, ground-glass opacity, fibrosis and micronodules. The Completed Local Binary Patterns (CLBP) descriptor associated with SVM classifier were used to obtain preliminary results.

II. Related Work

This section presents the recent work in classification of pulmonary patterns. Several types of features have been proposed for characterizing various lung disease patterns, and extracted from Regions of Interest (ROIs) and Volumes of Interest (VOIs). To classify the lung patterns, some authors used private images and others used the public database provided by Depeursinge et al. [3], which is also adopted in our study.

Anthimopoulos *et al.* [5] proposed a method for classification of Interstitial Lung Diseases (ILD), using local 2D discrete cosine transform (DCT) and random forest (RF) classification. The gray-level histogram values of the original image were also used to formed the feature vector. The method proposed by Dash et al. [6] used features extracted from Discrete Wavelet Transform (DWT) and two classifiers are trained, which are fused to obtain the final decision. A new sparse representation based method to classify Diffuse Lung Diseases patterns (DLD) was presented by Zhao et al. [7]. After extracting the local features from the VOIs, an overcomplete dictionary was learned using Singular Value Decomposition (K-SVD) algorithm,

and the descriptors were generated according to the dictionary and original feature vectors. Xu *et al.* [8] presented a bag-of-features based method which combined both the original CT values and eigenvalues of Hessian matrix. A new classification method of lung tissues was presented by Song et al. [9]. They proposed Rotation-invariant Gabor-LBP (RGLBP) texture and Multi-coordinate Histogram of Oriented Gradients (MCHOG) gradient descriptor, combined with intensity features. In addition, a new patch-adaptive sparse approximation (PASA) method was designed based on reference image patches. Li et al. [10] created a new image patch classification method, based on fully automatic feature learning. Firstly, feature extractors of different sizes were learned using the Gaussian Restricted Boltzmann Machine (GRBM) method. Then, the image feature vectors were obtained by convolving the feature extractors with the image patches. Depeursinge et al. [11] proposed a near-affine-invariant set of texture features to classify five types of lung tissues. The texture descriptors were based on Wavelet Transforms and the Gray-Level Histogram (GLH). In previous similar work, Malone et al. [12] proposed to classify body areas to perform a different lung segmentation, with the following lung patterns: normal tissue, emphysema and fibrosis. The method selected features among gray-level histogram, fourier transform, fractal and autocorrelation measures.

Table I summarizes the database used for each related work, as well as the overall results obtained. The average F-score reported by Anthimopoulos *et al.* [5] is defined in Equation 1. Definitions of the other metrics reported in the literature (sensitivity, accuracy and precision), as well as the specificity measure can be found in Section IV, since they were also used to evaluate this experiment.

Table I
SUMMARY OF RELATED WORK

Work	Database	Results
Anthimopoulos et al. [5]	Public - 2503 ROIs	Average F-score of 89%
Dash et al. [6]	Private - 100 ROIs	Overall accuracy of 95%
Zhao et al. [7]	Private - 2360 VOIs	Overall accuracy of 95.4%
Xu et al. [8]	Private - 3009 VOIs	Overall accuracy of 93.18%
Song et al. [9]	Public - 23731 ROIs	Overall precision of 80.7%
Li et al. [10]	Public - 16220 ROIs	Overall sensitivity of 74.2%
Depeursinge et al. [11]	Public - 17848 ROIs	Overall sensitivity of 76.9%
Malone et al. [12]	Private - 852 ROIs	Overall sensitivity of 89.5%

$$F_{avg} = \frac{1}{M}\sum_{c=1}^{M} F_c \tag{1}$$

where *M* is the number of of classes and F_c is the F-score for class c, defined as:

$$F_c = 2 \cdot \frac{precision_c \cdot sensitivity_c}{precision_c + sensitivity_c} \tag{2}$$

III. MATERIALS AND METHODS

A. Dataset

In this study, we used the publicly available database of ILD cases provided by Depeursinge *et al.* [3], which contains 113 sets of HRCT images of 512×512 pixels in DICOM format. Lung masks are available for each case. The database also provides annotated ROIs of 17 tissue patterns, including normal tissue. Among the 17 available tissues, five commonly seen lung patterns were selected: normal lung (N), emphysema (E), ground-glass opacity (GG), fibrosis (F) and micronodules (M).

The annotated ROIs were subdivided into half-overlapping blocks of 32×32 pixels, which have the best tradeoff between classification performance and localization [11]. The consolidation pattern was not considered since there were not sufficient extracted blocks (61 blocks).

In order to extract blocks belonging to non-pulmonary regions (e.g. fat and bone), the following technique was adopted: using the lung masks provided by the database, a morphologic dilation was applied, defined by $\delta^{(B)}(X)$ [13], where X is the lung mask image and B is a flat ellipse-shaped structuring element with a fixed radius of 5 pixels. Thus, we obtain the ROI of non-lung (R_{NL}), which is the dilated area that does not belong to the lung mask ($R_{NL} = \delta^{(B)}(X) - X$). We decided to set this area as the non-lung (NL) ROI because it contains more variation for being connected to the lung borders. After that, we extracted non-overlapping blocks of 32×32 pixels. Figure 1 shows the method of extraction of non-lung blocks. A total of 70000 blocks were extracted, but we randomly selected only 3000 blocks of non-lung to be used in the experiment. This is an intermediate number that was chosen based on the average number of extracted blocks per class from the lung tissues (see Table II).

Furthermore, for the blocks extraction, at least 75% of the pixels need to belong the ROIs. In total, HRCT image series of 91 patients were used to evaluate the performance of the proposed method. Examples of extracted blocks are presented in Figure 2.

A total of 20540 blocks were used in this experiment. Table II summarizes the total the number of blocks for each tissue type. All blocks were saved in DICOM format, to preserve the original values.

Table II
SUMMARY OF THE DATASET

Pattern	Number of blocks
Non-lung (NL)	3000
Normal (N)	5733
Emphysema (E)	1017
Ground-glass (GG)	1942
Fibrosis (F)	2736
Micronodules (M)	6112

Figure 1. Method of extraction of non-lung blocks, where (a) original image, (b) lung mask (X), (c) dilated lung mask ($0\delta^{(B)}(X)$) and (d) resulting image, where the gray part is the non-lung region ($R_{NL} = \delta^{(B)}(X) - X$).

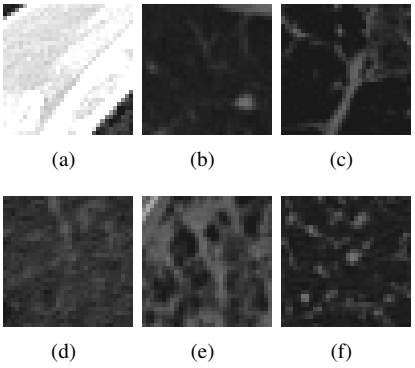

Figure 2. Example of extracted blocks of (a) non-lung (b) normal lung, (c) emphysema, (d) ground-glass opacity, (e) fibrosis and (f) micronodules.

It is important to observe that the aim of only labelling blocks with at least 75% of the ROI is to obtain good examples of the pattern. This does not reflets a real situation where, in the analysis of the lung CT images, a region of 32×32 pixels might contain more than one lung tissue pattern.

B. Completed Local Binary Pattern

Several variants of the Local Binary Pattern (LBP) descriptor have been proposed in the literature, such as the derivative-based LBP [14], dominant LBP [15], the center-symmetric LBP [16], and the completed LBP (CLBP) [17]. The LBPs were used as texture features to classify subtypes of emphysema [18]–[20], and a variation of LBP was proposed by Song et al. [9] to recognize lung patterns.

The CLBP method was proposed by Guo *et al.* [17] and it provides a complete modeling of LBP, representing a local region by its center pixel and a local difference sign-magnitude transform (LDSMT).

For a given central pixel g_c, the method calculates the difference between g_c and its P circularly and evenly spaced neighbours g_p, defined by $d_p = g_p - g_c$. This difference is decomposed into two components: sign, defined as $s_p = sign(d_p)$, and magnitude, defined as $m_p = |d_p|$.

To represent the original image, we use the center gray level (C) and the local difference, decomposed by the sign (S) and magnitude (M). Then, the operators CLBP_C, CLBP_S and CLBP_M are proposed to code the C, S and M features, respectively, and the combination of these operators forms the CLBP feature map of the original image.

The CLBP_S operator corresponds to the original LBP operator, whereas the CLBP_M operator is coded according to Equation 3 to make it consistent with that of CLBP_S:

$$\begin{aligned} CLBP\_M_{P,R} &= \sum_{p=0}^{P-1} t(m_p - c)2^p, where \\ t(x,c) &= \begin{cases} 1, & x \geq c \\ 0, & x < c \end{cases} \end{aligned} \tag{3}$$

where R is the radius of the neighbourhood and c is a threshold to be determined adaptively, which is originally defined as the mean value of m_p from the whole image.

Finally, the central gray level is coded as CLBP_C according to Equation 4:

$$\begin{aligned} CLBP\_C_{P,R} &= t(g_c - c_I), where \\ t(x,c_I) &= \begin{cases} 1, & x \geq c_I \\ 0, & x < c_I \end{cases} \end{aligned} \tag{4}$$

where c_I is set as the average gray level of the whole image.

All the three code maps are in binary format so that they can be easily combined to form the final histogram. A rotation invariant version of CLBP_M can be achieved and the histograms of codes can be combined in different schemes. In this experiment, the combination used to generate the histogram was the CLBP_S/M/C, which is the CLBP scheme that presented the best results in Guo et al. [17].

IV. Experimental Results and Discussion

The dataset was divided using a five-fold cross validation method. The folds were split based on the patients, ensuring that all blocks belonging to a patient remain in the same fold, preventing training and testing with the same patient and avoiding the over-fitting for the test images.

We evaluate two different combinations of the CLBP_S/M/C configuration. The first was $CLBP\_SMC^{u2}_{(P,R)}$ that refers to the CLBP uniform pattern and the second was $CLBP\_SMC^{riu2}_{(P,R)}$ that is the

rotation invariant uniform pattern. Both variations were applied using the values $(8,1)$ and $(8,2)$ for the (P,R) parameters. Thus, four different CLBP combinations were tested.

Each attribute from the feature set was normalized in the range [-1, +1]. We used the SVM classifier with a Gaussian kernel and a one-versus-one approach. SVMs have shown to be the best classifier in recognizing lung patterns [21]. Furthermore, the best parameters for the classifier were determined through a grid-search method for each fold.

The performance of the classification is measured by sensitivity, precision, specificity and accuracy, specified by the following equations:

$$sensitivity = \frac{TP}{TP+FN} \tag{5}$$

$$precision = \frac{TP}{TP+FP} \tag{6}$$

$$specificity = \frac{TN}{TN+FP} \tag{7}$$

$$accuracy = \frac{TP+TN}{TP+FP+FN+TN} \tag{8}$$

where FP, FN, TP, and TN stand for False Positive, False Negative, True Positive, and True Negative, respectively. In addition, ROC curves and the Area Under the Curve (AUC) for each classification were calculated. Performance measures of the blockwise classification are shown in Table III. Figure 3 shows the magnified graphic for the ROC curves and allows to visualize the best feature extractor configuration.

Table III
OVERALL RESULTS FOR THE BLOCKWISE CLASSIFICATION (IN %)

Classifier	Sensitivity	Precision	Specificity	Accuracy	AUC
$CLBP\_SMC^{riu2}_{(8,2)}$	78.99	75.95	93	95.55	93.4
$CLBP\_SMC^{riu2}_{(8,1)}$	75.29	70.84	91.76	94.82	91.2
$CLBP\_SMC^{u2}_{(8,2)}$	74.18	70.76	91.39	94.51	91.1
$CLBP\_SMC^{u2}_{(8,1)}$	72.06	67.89	90.69	94.12	90.1

By looking at the overall results (Table III) and the ROC curves (Figure 3), one can see that the best results were achieved with $CLBP\_SMC^{riu2}_{(8,2)}$, and the worst performance was with the $CLBP\_SMC^{u2}_{(8,1)}$ classifier. The remaining classifiers achieved very similar results. The confusion matrix of the best CLBP classifier is presented in Table IV.

Table IV shows that most of the confusions occurred between emphysema and normal, ground-glass and normal, and ground-glass and fibrosis. The inter-class confusions can be explained by the fact that as emphysema and normal tissue can appear quite dark in the overall lung field, it could

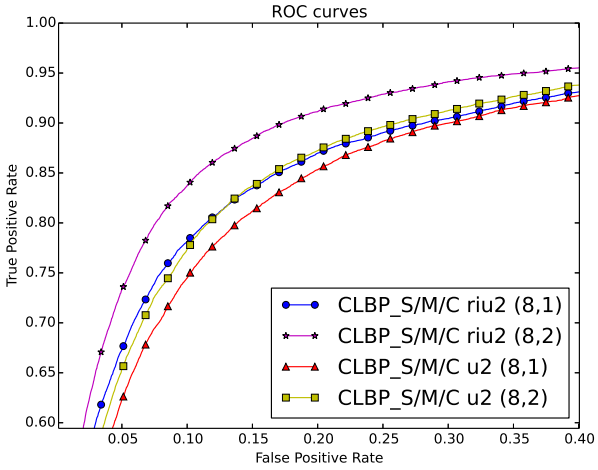

Figure 3. ROC curves for CLBP_SMC classifiers

Table IV
CONFUSION MATRIX FOR THE BEST CLBP_SMC CONFIGURATION IN %

Class	Predicted					
	NL	N	E	GG	F	M
NL	97.5	0.7	0.17	1.37	0.23	0.03
N	0.68	79.98	0.78	7.01	0.72	10.83
E	2.46	19.96	57.13	5.51	10.91	4.03
GG	3.5	24.46	0.26	39.8	23.43	8.55
F	0.58	1.1	1.86	15.1	77.6	3.76
M	0.02	9.62	0.44	1.42	2.81	85.68

be difficult to differentiate the parenchyma details of these two patterns and, regarding the ground-glass opacity, it can show relatively high densities, looking similar to fibrosis [9]. On the other hand, emphysema and fibrosis contain more irregular local structures, showing large intra-class variation. Moreover, healthy tissue does not possess a single uniform texture, depending on the age or the smoking history of the patient [3] and the variable appearance of vessels and bronchioles [12].

The overall results for $CLBP\_SMC^{riu2}_{(8,2)}$ can be seen in Table V. The classification results achieved by normal lung tissue, fibrosis and micronodules were similar to the literature, in which the micronodules category obtained the highest rate among some studies that used the same database (see [9]–[11]). Normal lung category achieved better sensitivity than the presented in [10], [11], but still did not achieved scores as reported in [9].

Regarding the non-lung pattern, a sensitivity of 97.5% was achieved for the blockwise classification, and 99.15% for the lung tissue patterns. Malone et al. [12] obtained 98% of sensitivity for the non-lung category, but it is important to note that they used a private dataset.

Table V
RESULTS OF THE BLOCKWISE CLASSIFICATION FOR THE BEST CLBP_SMC CONFIGURATION IN %

	Sensitivity	Precision	Specificity	Accuracy
Non-lung	97.5	95.15	99.15	98.91
Normal	79.98	77.69	91.11	88
Emphysema	57.13	81.37	99.32	97.23
Ground-glass	39.8	43.62	94.63	89.44
Fibrosis	77.6	72.98	95.59	93.19
Micronodules	85.68	84.89	93.54	91.2

V. CONCLUSION

Diagnosis of lung diseases is usually accomplished by analyzing CT scans searching for abnormal characteristics. In recent years, many studies about classification of lung diseases have been developed, but they have shown difficulty in differentiating certain pulmonary patterns, which also cause confusion among specialists due to their similarity.

This paper presented initial results in classification of texture patterns from HRCT of the lung using the CLBP descriptor with a SVM classifier. Among the pulmonary patterns, we also classify body areas outside the lungs, in order to perform a coarse lung segmentation. The rotation-invariant uniform version of CLBP_S/M/C showed the best results, with the parameters $P = 8$ and $R = 2$.

Classification results comparable to the literature were achieved for normal lung tissue, fibrosis and micronodules, in which the micronodules category obtained the highest rate among some studies that used the same database. However, emphysema and ground-glass categories obtained the lowest results reported in the literature. Our study demonstrated this very clearly through a complete evaluation comparing the main measures of accuracy described in the literature. Moreover, we achieved 97.5% of sensitivity in the blockwise classification for the non-lung pattern.

The main drawback of the proposed method is that it performs multiple misclassifications between the classes emphysema and normal, ground-glass and normal, and ground-glass and fibrosis. This is one limitation of using only texture descriptors. Some regions of the lung do not possess a homogeneous texture.

Future work will focus on the analysis and quantification of lung disease patterns. At the present moment, we are simply abstractly comparing noncontiguous blocks. In order to improve the results and to minimize the errors, we will develop a methodology that combines the results of multiple classifiers with CLBP (e.g. gray-level histogram, top-hat analysis). These classifiers will be able to produce a posterior probability $P(class|input)$ which can be used to determine the chance of a given region of the lung to be abnormal. We can also work with different block sizes to classify the CT images, since a block of 32×32 pixels may not belong to a sigle class. Finally, it will be possible to perform the lung segmentation before the lung tissue classification of the whole HRCT image.

The complete implementation of the method presented here can be found at http://web.inf.ufpr.br/vri/alumni/2015-LuizaDriBagesteiro-Msc.

REFERENCES

[1] I. Sluimer, A. Schilham, M. Prokop, and B. Van Ginneken, "Computer analysis of computed tomography scans of the lung: a survey," *Medical Imaging, IEEE Transactions on*, vol. 25, no. 4, pp. 385–405, 2006.

[2] U. Bagci, M. Bray, J. Caban, J. Yao, and D. J. Mollura, "Computer-assisted detection of infectious lung diseases: A review." *Comp. Med. Imag. and Graph.*, vol. 36, no. 1, pp. 72–84, 2012.

[3] A. Depeursinge, A. Vargas, A. Platon, A. Geissbuhler, P.-A. Poletti, and H. Mller, "Building a reference multimedia database for interstitial lung diseases," *Computerized Medical Imaging and Graphics*, vol. 36, no. 3, p. 227238, 2011.

[4] S. O. Park, J. B. Seo, N. Kim, S. H. Park, Y. K. Lee, B.-W. Park, Y. S. Sung, Y. Lee, J. Lee, and S.-H. Kang, "Feasibility of Automated Quantification of Regional Disease Patterns Depicted on High-Resolution Computed Tomography in Patients with Various Diffuse Lung Diseases," *Korean Journal of Radiology*, vol. 10, no. 5, p. 455463, 2009.

[5] M. Anthimopoulos, S. Christodoulidis, A. Christe, and S. Mougiakakou, "Classification of interstitial lung disease patterns using local dct features and random forest," in *Engineering in Medicine and Biology Society (EMBC), 2014 36th Annual International Conference of the IEEE*, Aug 2014, pp. 6040–6043.

[6] J. Dash, S. Mukhopadhyay, M. Garg, N. Prabhakar, and N. Khandelwal, "Multi-classifier framework for lung tissue classification," in *Students' Technology Symposium (TechSym), 2014 IEEE*, Feb 2014, pp. 264–269.

[7] W. Zhao, R. Xu, Y. Hirano, R. Tachibana, and S. Kido, "Classification of diffuse lung diseases patterns by a sparse representation based method on hrct images," in *Engineering in Medicine and Biology Society (EMBC), 2013 35th Annual International Conference of the IEEE*, July 2013, pp. 5457–5460.

[8] R. Xu, Y. Hirano, R. Tachibana, and S. Kido, "A bag-of-features approach to classify six types of pulmonary textures on high-resolution computed tomography," *IEICE Transactions*, vol. 96-D, no. 4, pp. 845–855, 2013.

[9] Y. Song, W. Cai, Y. Zhou, and D. Feng, "Feature-based image patch approximation for lung tissue classification," *Medical Imaging, IEEE Transactions on*, vol. 32, no. 4, pp. 797–808, April 2013.

[10] Q. Li, W. Cai, and D. Feng, "Lung image patch classification with automatic feature learning," in *Engineering in Medicine and Biology Society (EMBC), 2013 35th Annual International Conference of the IEEE*, July 2013, pp. 6079–6082.

[11] A. Depeursinge, D. V. D. Ville, A. Platon, A. Geissbhler, P.-A. Poletti, and H. Mller, "Near-affine-invariant texture learning for lung tissue analysis using isotropic wavelet frames." *IEEE Transactions on Information Technology in Biomedicine*, vol. 16, no. 4, pp. 665–675, 2012.

[12] J. Malone, J. Rossiter, S. Prabhu, and P. Goddard, "Identification of disease in ct of the lung using texture-based image analysis," in *Signals, Systems and Computers, 2004. Conference Record of the Thirty-Eighth Asilomar Conference on*, vol. 2, Nov 2004, pp. 1620–1624 Vol.2.

[13] P. Soille, *Morphological Image Analysis: Principles and Applications*, 2nd ed. Heidelberg: Springer, 2003.

[14] X. Huang, S. Li, and Y. Wang, "Shape localization based on statistical method using extended local binary pattern," in *Multi-Agent Security and Survivability, 2004 IEEE First Symposium on*, Dec 2004, pp. 184–187.

[15] S. Liao, M. Law, and A. Chung, "Dominant local binary patterns for texture classification," *Image Processing, IEEE Transactions on*, vol. 18, no. 5, pp. 1107–1118, May 2009.

[16] M. Heikkilä, M. Pietikäinen, and C. Schmid, "Description of interest regions with local binary patterns," *Pattern Recogn.*, vol. 42, no. 3, pp. 425–436, Mar. 2009.

[17] Z. Guo, D. Zhang, and D. Zhang, "A completed modeling of local binary pattern operator for texture classification," *Image Processing, IEEE Transactions on*, vol. 19, no. 6, pp. 1657–1663, June 2010.

[18] L. Sørensen, S. B. Shaker, and M. Bruijne, "Texture classification in lung ct using local binary patterns," in *Proceedings of the 11th international conference on Medical Image Computing and Computer-Assisted Intervention - Part I*, ser. MICCAI '08. Berlin, Heidelberg: Springer-Verlag, 2008, pp. 934–941.

[19] L. Sorensen, S. Shaker, and M. de Bruijne, "Quantitative analysis of pulmonary emphysema using local binary patterns," *Medical Imaging, IEEE Transactions on*, vol. 29, no. 2, pp. 559–569, Feb 2010.

[20] M. Gangeh, L. Srensen, S. Shaker, M. Kamel, M. de Bruijne, and M. Loog, "A Texton-Based Approach for the Classification of Lung Parenchyma in CT Images," in *Medical Image Computing and Computer-Assisted Intervention MICCAI 2010*, ser. Lecture Notes in Computer Science, T. Jiang, N. Navab, J. P. Pluim, and M. A. Viergever, Eds. Springer Berlin Heidelberg, 2010, vol. 6363, p. 595602.

[21] A. Depeursinge, J. Iavindrasana, A. Hidki, G. Cohen, A. Geissbhler, A. Platon, P.-A. Poletti, and H. Mller, "Comparative performance analysis of state-of-the-art classification algorithms applied to lung tissue categorization." *J. Digital Imaging*, vol. 23, no. 1, pp. 18–30, 2010.